Received 16 March 2023; accepted 3 April 2023. Date of publication 10 April 2023; date of current version 21 April 2023.

Digital Object Identifier 10.1109/OJAP.2023.3265691

Indirect Applications of Additive Manufacturing for Antennas

JONATHAN D. LUNDQUIST (Member, IEEE), LAUREN LINKOUS (Member, IEEE), UMAR HASNI (Member, IEEE), AND ERDEM TOPSAKAL (Senior Member, IEEE)

Department of Electrical and Computer Engineering, Virginia Commonwealth University, Richmond, VA 23220, USA

CORRESPONDING AUTHOR: J. D. LUNDQUIST (e-mail: lundquistjd@vcu.edu)

ABSTRACT We report the fabrication methodology of stereolithography (SLA) printed molds for metal and resin cast antennas. In the first method, a conical horn created using metal cast molds printed from a glass-filled resin utilizes a casting technique allowing for low-cost 3D printing to fabricate metal antennas, reducing the losses incurred by metallized plastics, while still producing complex geometries quickly. This metal cast conical horn is compared to a horn constructed using a more traditional 3D printing method. The second casting method demonstrates the interchangeability between creating parts via SLA printing with a glass-filled resin and using the same resin cast into a reusable Polydimethylsiloxane (PDMS) mold. We demonstrate this method by casting an interchangeable slug for a capacitively coupled, mechanically reconfigurable disk loaded monopole. Simulated and experimental data are presented for S_{11}, and Gain. Simulated BW, directivity, gain and efficiency as a function of frequency are presented. The results indicate that the 3D printed metal casting process produces antennas with a higher gain and lower return loss than metallized resin antennas. The method is suitable for difficult geometries requiring resolution of at least 50 μm. The capacitively coupled disk loaded monopole demonstrates the versatility of 3D printing in antenna fabrication.

INDEX TERMS 3D printed antenna, disk loaded monopole, conical horn, metal casting, resin casting.

I. INTRODUCTION

ANTENNAS fabricated using additive manufacturing technologies, such as 3D printing, present unique opportunities on which to capitalize and, as in any new technology, some challenges. The 3D printing process allows for geometries that would otherwise be very difficult to achieve and supports rapid prototyping of components [1]. 3D manufacturing technology has led to the realization of mechanically configurable, liquid metal antennas embedded in 3D printed structures [2]. The ability to easily prototype and manufacture these more difficult to fabricate designs make a compelling argument for further research in elements made possible by 3D printing technologies. Included in the challenges of these approaches, antennas printed from plastics and resins, such as acrylonitrile butadiene styrene (ABS) and metallized with metallic inks, often have lower efficiency because of low conductivity [3], [4]. Other materials commonly used in printing metallized antennas on dielectric supports or substrates are polylactic acid (PLA) extrusion printers and resins on stereolithography (SLA) printers. These suffer the same performance issues seen in other antennas in this class. In [5], the return loss for two identical patch antennas is compared, where one is made from copper and the other is made from PLA. The copper antenna has a return loss of −25 dB, while the PLA antenna has a return loss of −12.5 dB. In another paper [6], an SLA printer was used to print horn antennas which were electroplated with copper. These were compared to solid metal horn antennas made on a lathe. The metal antenna's gain was found to be 0.5 dB higher than the resin antenna's gain across the design spectrum.

There are a few fabrication methods in which 3D printing has been used to produce antennas thus far, each with their own hurdles to widespread adoption. One technique, touched on previously, entails printing a support structure or substrate out of a dielectric material such as ABS and then metallizing it using metallic inks [7]. Alternatively, an antenna can be printed entirely out of a metal using a metal 3D printer [8]. However, this approach can be costly. In one report, a dual extruder was used with a dielectric filament and

FIGURE 1. Commercial off-the-shelf metal cast, aperture matched corrugated conical horn, with mold seam annotated.

a graphene infused conducting filament to 3D print antennas in a one step process [9], but the fabricated antennas suffered from the same performance problems as metallized dielectric antennas. Liquid metals such as Gallium, Mercury and conductive liquid solutions have been used in 3D printed structures for mechanically reconfigurable antennas [10]. Another approach is to print dielectric rod antennas out of ABS plastic [11]. These approaches are not dissimilar to our disk loaded monopole, however our approach is designed for at scale production.

While fabrication methods discussed in the previous paragraphs are already in use for 3D printed antennas, direct printing of metallic structures using a metal 3D printer can be expensive [12], and other methods suffer in performance. Fortuitously, high temperature resins provide a pathway by supporting production of low temperature metal casting molds on stereolithography 3D printers. The produced molds can then be used to create purely metallic antennas at a lower cost than is commonly seen in 3D metal printing. One resin that is suitable for the casting process is Formlabs' Rigid 10K, which has a heat deflection temperature (HDT) of 218°C at 0.45 MPa [13]. The HDT of Rigid 10K is above the melting point for many Bismuth-Tin alloys [14]. The crossing of thresholds between the resin HDT and Bismuth-Tin melting temperature is an ideal combination of materials for the metal casting fabrication process. As a result of Bismuth-Tin alloys and Formlabs' resins being relatively inexpensive, the material combination employed also provides for an inexpensive method of fabrication for difficult topologies, while retaining most of the benefits of constructing solid metal antennas.

While the casting process presented in this work resembles closely the metal-based casting integral to many manufacturing processes [15], [16], [17], [18], [19], [20], the use of 3D printing technology with a temperature tolerant resin addresses several common challenges. What is evident from products like the aperture matched corrugated conical horn in Figure 1, is that metal casting is already used in antenna production; however, there is little indication in the literature that much research has assessed this manufacturing method's impact on antenna performance, and where it has, the performance difference is significant [18]. Common casting techniques include gravity casting, high-pressure die-casting, low-pressure casting [15], sand casting, and lost wax casting [17]. Quality of the mold materials and mold cleanliness are challenges of most techniques [16], while methods for high-pressure die-casting, low-pressure casting, and lost wax casting are complex processes with four or more steps [17], [19]. The method presented in this paper is a type of gravity casting, which has the advantage of process simplicity, but is typically plagued by defects originating from bifilm oxides, which can be exacerbated by pouring velocity, direction of fill, and the rate of metal solidification [20]. We solve this problem by using a glass-filled resin with low thermal conductivity and with temperature deflection higher than the Bismuth-Tin alloy, allowing the mold to be used as a crucible thereby eliminating the bifilm oxides that lead to material defects. This process has two benefits: If the molten alloy is poured into the mold, the creation of bifilm, commonly seen as 'skin' on molten metals, will not be folded into the alloy during the cooling process; secondly, rather than being fed in through a vent, the metal can be fully melted within the mold, lowering process complexity. Using this process, and skipping the addition of materials such as wax in the pre-casting stages, reduces not just the complexity of the process, but also lessens issues such as incomplete wax removal that could lead to voids if the hot alloy reacts with the residue to create gasses rather than burning it off. As additive manufacturing, especially SLA printing, does not suffer from the same geometric complexity bounds as other manufacturing (and casting) techniques, the precision of 3D printing in this metal casting process allows for the precise placement of vents in locations that other methods may struggle to recreate. Furthermore, the resolutions from SLA printing minimize, and potentially eliminate, the need for machining as a major part of post-processing the metal casting process.

In addition to being used to create the molds for metal casting, SLA printer resins can be poured into PDMS molds and cured using the same ultraviolet light post-process as if they had been printed. The process presented in this paper uses PDMS due to its well-researched use as a non-reactive silicate-based mold material and ability to achieve feature resolutions on the scale of 40 nm [21]. With this, the creation of resin-based parts can be done in a time trivial when compared to the time needed for additive manufacturing methods.

In this paper, we present an inexpensive fabrication method which employs metal casting using 3D printed molds to prototype complex geometries without sacrificing antenna performance. Using this fabrication method, we present a conical horn cast from Bismuth-Tin alloys into a mold created with the glass-based Formlabs' Rigid 10K resin. We also demonstrate the efficacy of using a silicate-based polymer, in this case PDMS, to create reusable molds for casting the same Formlabs' Rigid 10K resin to create the

internal components of a capacitively coupled, mechanically reconfigurable, disk loaded monopole. The conical horn produced in this paper is compared to the more traditional 3D printed antenna fabrication method of metalizing a 3D printed dielectric structure with conductive ink.

II. 3D PRINTED METAL CASTING METHODOLOGY

The conical horn presented here was constructed from cast metal (60Sn-Bi40). In this section, we will break down the steps of this methodology to include materials used, aspects of mold design, melting, pouring, and metal extraction. Taking advantage of the radially symmetric shape of the horn allows for the demonstration of two slight variations of this metal casting fabrication method.

A. MATERIAL SELECTION

As touched on briefly in the introduction, the Rigid 10K resin was chosen for the mold material owing to its high heat deflection temperature and low thermal conductivity. The HDT of Rigid 10K resin at atmospheric pressure is higher than the melting temperature of Bismuth-Tin alloys [22]. As a result of this higher HDT, the Rigid 10K resin, which can be printed with a high degree of accuracy on Formlabs' 3D printers, is an ideal mold material for casting Bismuth-Tin into. The properties of Rigid 10K allow for the 60Sn-40Bi alloy to be poured into the molds without damaging them and provides sufficient thermal insulation so that air can escape from the molds before the metal solidifies. Considering these materials, with the HDT of Rigid 10K being higher than the melting point of the Bismuth-Tin, it is also possible to melt the metal inside of the two-part mold presented, eliminating the need for pouring all together. This approach of using the mold as a crucible is not possible in sand casting, or other metal casting processes using compacted materials, due to the hard, unmelted alloy deforming the mold. In both approaches used in this section, air evacuation is important to achieve a smooth, non-porous surface, which could alter the functionality of an antenna. The ability to print the molds from Rigid 10K supports the option for molds to be manufactured with the 25 micron resolution available in the Form 3B printer [23].

B. MOLD DESIGN

The mold design is dependent on the geometry of the antenna. For some geometries it is trivial to remove the metal from the mold. For others, the mold may need to be designed for ease of shattering, so that the metal is not impinged during removal, but strong enough to endure the forces present due to the difference in contraction of the mold and metal materials as the metal cools. While Rigid 10K is brittle and will shatter with impact, it is not so brittle that it is trivial to shatter without potentially damaging the underlying metal. Designed weak points in the mold can improve ease and success of mold removal. Topologies with a high surface to volume ratio, and surfaces where the metal surrounds the mold material were found to require mold shattering. The need to shatter the mold in the latter case occurs because the metal appears to contract faster than the mold material as it cools, placing significant pressure on the mold, when it is cast around it. Mold release, or other agents to make removal of the cast horn easier, was not used in either of the fabrication variations presented here. To remove residue left over from the SLA print wash and curing process, a high-grit sandpaper was lightly run over the mold, but the mold was not sanded as part of the post processing to change dimensionality or features.

C. MELTING AND POURING

To melt the Bismuth-Tin metal, ingots were placed in a steel dish which was used as a crucible because of its high melting temperature. This dish was placed on a commonly available hot plate capable of reaching 232°C. The resin molds were heated on the hot plate at the same time so that there would be no thermal shock when the metal was poured into the mold. A Pyrex lid was placed on the dish during the heating process. The temperature was raised in increments of 50°C every 30 minutes to minimize thermal stress and thus prevent premature shattering of the molds. As the Bismuth-Tin melted, it was occasionally agitated to ensure all the material had liquefied. After the Bismuth-Tin was poured, the hot plate was turned off and the mold remained in the hot plate while it was allowed to cool naturally.

In a separate instance, the bottom half of the mold was used as the crucible to melt the Bismuth-Tin to reduce the amount of bifilm oxides folded into the cooling metal. The alloy and mold were both brought to a temperature of 173°C following the previously mentioned procedure. Figure 6 shows the liquified metal in the bottom half of the mold. The final horn is indistinguishable from the horn made using the pour process.

D. METAL EXTRACTION

For molds that could be removed without shattering it is not necessary to wait until room temperature for removal. As seen in Figure 2, the cast Bismuth-Tin transitions to a solid state well above the ambient room temperature. However, for geometries that require shattering, it may be difficult to remove the mold while it is hot to the touch. It was found that wet sanding the inside of the molds with high grit sandpaper before pouring could aid in ease of removal by smoothing or removing residue left from print post-processing. For molds that do not require shattering a light tap was all that was needed to remove the cast metal. Molds that required shattering were removed with a chisel and hammer, taking care to avoid hitting the metal on the other side. This process was tested with the creation of a conical horn, comparing it to more traditional 3D printing fabrication methods. In later sections, a detailed analysis of antenna design and measurements for this topology will be discussed.

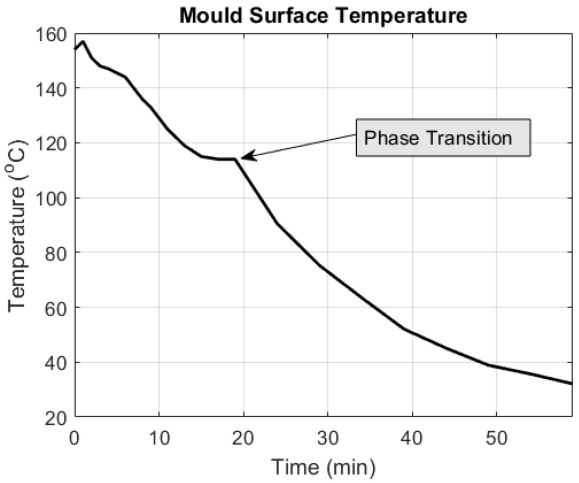

FIGURE 2. Temperature of the cast Bismuth-Tin in the Rigid 10K SLA printed molds measured with a FLIX E4 Thermal Imaging Camera as it cooled to room temperature.

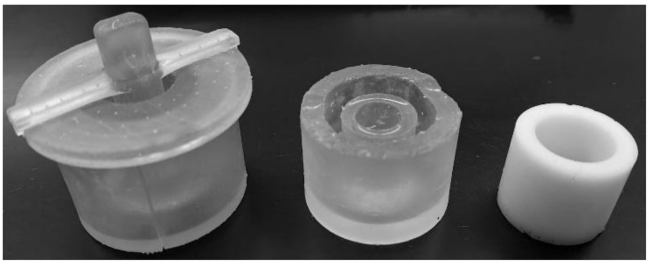

FIGURE 3. From left to right; the multi-piece positive mold made from Formlabs' BioMed Clear resin, the negative mold made from PDMS, and the final part cast from Formlabs' Rigid 10K resin.

III. RESIN CASTING METHODOLOGY

Within this section is presented the methodology for creating equivalents of SLA printed pieces through liquid resin and reusable molds. The geometrically simple example shown here is one of several pieces featured in an antenna topology discussed later in this paper that work well with both small-batch and scalable manufacturing methods. The final, resin cast parts are created from a glass-filled resin, Formlabs' Rigid 10K, and after post processing are identical to the parts created on the Formlabs Form 3B and Form 3BL printers. In this section we discuss the process for creating the pieces for the positive mold, creating the negative PDMS mold, and finally casting the SLA printer resin into the desired antenna part. The results of the three-part process of molds and final resin cast part are shown in Figure 3. Post processing for the resin parts differs little from traditional processing of SLA parts using an isopropyl alcohol wash and UV curing following manufacturer instructions. Both molds are easily cleanable, do not require the use of a mold release agent, and are reusable. This section includes rationale for the materials used, the mold designs, and the casting process.

A. MATERIAL SELECTION

First, PDMS was selected to create the negative mold due to it being chemically inert, physically flexible, and resilient to permanent warping during part extraction. Other silicone-based mold creation methods were considered, but PDMS cures clear, which makes it possible to UV cure the cast resin through the negative mold without reducing efficiency. PDMS properties have also been well studied, and common issues with improper curing caused by contact with some 3D printing materials are documented [21], [24], [25]. According to the authors in [21], PDMS molds can have line features on the scale of 40 nm, which is more precise than the maximum resolution for current Formlabs' SLA printers (25 microns) and ensures that fine details will not be lost in the molding medium. The Rigid 10K resin, used to cast the part, did not bind to the PDMS mold during compatibility testing as it does to other SLA resins. There were also no observed curing inhibitions for the PDMS.

The multi-part positive mold was printed using Formlabs' BioMed Clear resin [26]. BioMed Clear is a medical-grade, rigid resin that prints clear even with wall thicknesses of multiple millimeters. It was a desirable choice for visually confirming proper air evacuation without disturbing the PDMS curing process. This biocompatible material prints with a resolution of 100 microns and is non-porous, reducing the difficulty of removing cast materials by providing a smooth surface. Rigidity, resolution, and resilience of the multi-part mold are discussed in the following sections.

B. MOLD DESIGNS

The positive mold was printed out of BioMed Clear resin in four parts; two identical pieces for the bottom cup, a lid with an attached positive mold of the antenna part to be cast in Rigid 10K, and an extra center insert used to make the center of the PDMS negative mold flexible for easier part extraction. This mold was designed so that all parts could be printed on the Form 3B at the same time and to minimize the amount of PDMS needed to create the negative. The mold was held together during air evacuation and curing with a piece of electrical tape wrapped around the circumference of the two bottom halves of the cup, but nothing was used to permanently connect any parts of the mold. Figure 4 shows the pieces and an assembled version of the mold.

The negative mold was made from the two-part SYLGARD 184 Silicone Elastomer Kit following manufacturer instructions. The mixture was poured into the assembled bottom cup of the positive mold, and air evacuated out with a hand pumped vacuum chamber. The lid and center insert were added last to minimize air pockets. Due to HDT limitations on parts printed from BioMed Clear [26], the negative mold was left to cure at room temperature for two days before the PDMS was extracted from the positive mold.

C. CASTING, CURING, POST PROCESSING

The pieces of the BioMed Clear positive mold were processed after printing on the SLA printer using a 99% isopropyl alcohol bath, rinsed with water, air dried, assembled, and then UV cured for one hour at 60°C following manufacturer recommendations. The mold is held together

FIGURE 4. The PDMS negative mold, and both assembled and disassembled positive molds 3D printed from BioMed Clear resin.

by an interference fit of the two halves of the bowl against the recession on the bottom side of the lid. By assembling the mold prior to curing, warping was minimal and consistent across parts. To prepare the mold for making the PDMS, a piece of electrical tape was wrapped around the circumference of the two bottom halves of the cup.

Due to the BioMed Clear resin having a max HDT of 67°C (at 0.45MPa) [26], the PDMS was left to cure in the positive mold for two days at room temperature as to not damage the structural integrity of the molds instead of using an oven to shorten the curing time. Formlabs has released a high temperature resin that prints semi-transparent with a HDT at 238 °C of 0.45 MPa [27], and it may be a suitable alternative for printing as opposed to BioMed Clear. When the PDMS was extracted from the positive mold, it was inspected for damage and rinsed with water to remove any residue.

The final antenna part was created by carefully pouring Rigid 10K resin into the negative mold. During several stages while being filled, the mold was tapped gently on the table to encourage air bubbles to float to the surface. When filled, the mold was immediately placed in the Formlabs' UV cure station while it was brought up to temperature, and cured for 40 minutes at 60°C.

When the part was successfully removed from the PDMS mold, it was washed in a 99% isopropyl alcohol bath for 15 minutes before being dried and inspected. The part was placed in the UV cure station for another 10 minutes at 60°C to dry further before 2500 grit sandpaper was used to remove the sharp edge left from the meniscus. For aesthetic purposes, the part can be wet sanded using a high grit sandpaper to make the top face match the sides that were cured against the PDMS, but this was not utilized. The mold shown in this section is reusable; the final antenna part was easily removed without the need for mold release agents, and any extra resin that was accidentally spilled on the mold during the filling process was allowed to cure and then flaked off.

TABLE 1. Relative permittivity measurements rigid 10K.

Resonant Frequency (GHz)	Patch Length (mm)	Calculated Relative Permittivity
6.41	12.16	3.30

IV. CONICAL HORN

A conical horn is one of two antennas presented as an example of the metal cast fabrication method. We show two variations of the metal cast fabrication method, pouring the molten alloy into the two-part mold and melting the alloy directly by using the bottom half of the mold as the crucible, which produces identical results. Conical horns are a common antenna that can be difficult to fabricate. The fabricated conical horns are to compare 3D printing fabrication methods, with the expectation that the metal cast horn will perform significantly better than a metallicized resin horn. Horn antennas can be an expensive antenna structure, but also have broad applications such as reflector feeds, cell tower antennas and metrology. Conical horns have the advantage of being able to be made on a CNC lathe, owing to their cylindrical symmetry, however the process could be made even less expensive and faster than that afforded by a lathe. The conical horn presented here is fabricated using two processes. The metal casting process described in Section II is used to fabricate the conical horn, as well as the more traditional method of 3D printing the antenna out of a dielectric and metallicizing it.

A. DESIGN AND CONSTRUCTION METHODS

The silver ink metallicized resin horn was printed from the same Formlabs' Rigid 10K resin used to make the mold for the metal cast antenna. The Rigid 10K resin was chosen because of its ability to withstand the temperature of the silver ink curing process. To design and simulate the antenna, we first had to determine the relative permittivity of the Formlabs' Rigid 10K resin and the resistivity of the Novacentrix HPS-FG181 ink used to metallize the antenna. A patch antenna was used to determine permittivity of the resin and it was found to be 3.3 (See Table 1), which was in the expected range, given the high glass content of this particular resin [13]. The expected resistivity of the Novacentrix silver ink for the recommended cure time of 30 minutes at 140°C was provided in correspondence from the manufacturer and was 34 $\mu\Omega$-cm.

The Form 3B printer has a build size of 145 mm by 145 mm [23]. The antenna design was restricted in size so that either fabrication process could be performed with only a single print. The initial design started with a conical waveguide that had a quarter-wave radius for 5 GHz in free space and a feed that was approximately a quarter-wave from the back wall. Simulations performed in HFSS and parametric sweeps were an integral part of the design process for the horn. These simulations were refined to include the known parameters of the material used in both horns. The

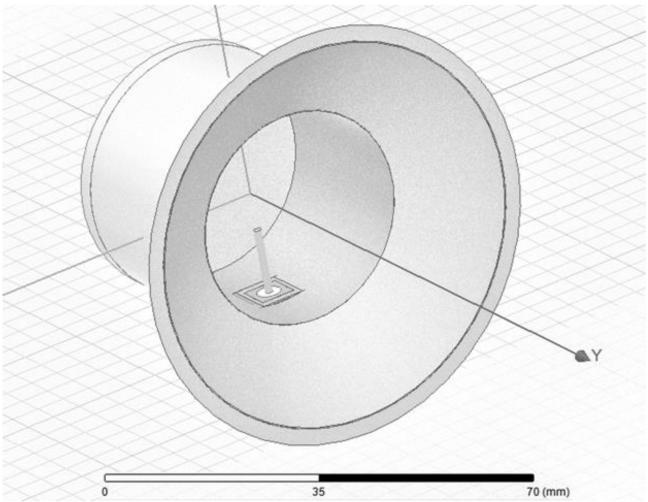

FIGURE 5. Conical Horn CAD model.

TABLE 2. Conical horn antenna dimensions.

Dimension	Distance (mm)
Total Length	42.3
Wall Thickness	3.0
Inner Radius	18.4
Feed Distance	15.7
Aperture Radius	33.0

horn and aperture were restricted to limit the size of the antenna and a parametric sweep was performed to fit the size parameters while also achieving a band of 5.3 GHz to 6.3 GHz. The resulting parameters can be seen in Table 2 and the CAD design can be seen in Figure 5.

The resin antenna was designed so that a standard SMA fitting with the pin extended can be used as the feed. This was secured in place with high temperature epoxy, so that the Novacentrix ink could be cured in contact with the fitting ground. The Novacentrix HPS-FG181 was applied by brushing a light coat onto the inside of the conical horn and curing the ink for 30 minutes at 140°C.

The metal cast antenna used a mold that was designed from the negative of the CAD model seen in Figure 5. The mold, seen in Figure 6 a, was designed such that metal would be poured in the bottom cup and the top cup inserted. Four clips were used to center the top portion of the mold in the bottom. Due to the top portion of the mold being buoyant in the Sn-Bi alloy, a ceramic weight (Figure 6 c) was used to hold down the top portion of the mold during the cooling process. Excess metal was allowed to overflow into the pan and was cut off around the edge during the cleanup process. The fabrication process of the metal cast conical horn was identical to that described in Section II.

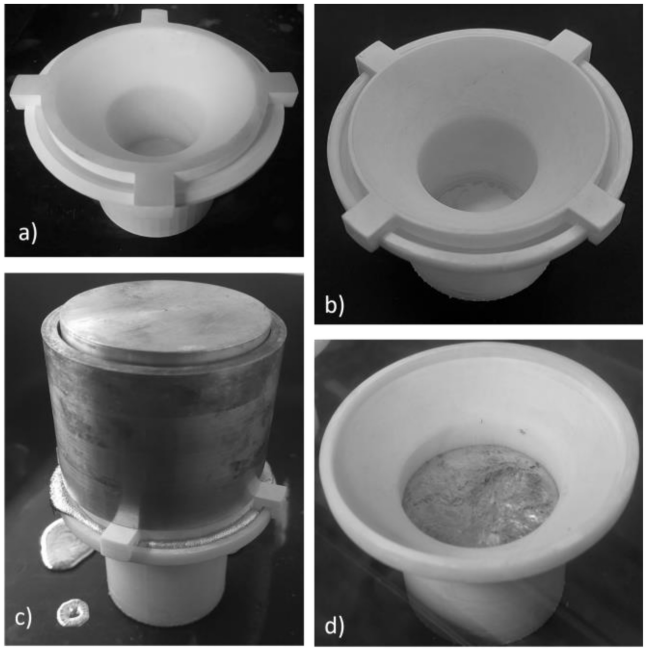

FIGURE 6. Metal cast conical horn molds and casting process - (a) The assembled mold used when fabricating via pouring the melted Sn-Bi alloy. (b) The assembled mold, with higher outer rim, used when melting the Sn-Bi alloy in the bottom mold. (c) Assembled mold with ceramic weight to keep the top half in place while cooling. (d) Sn-Bi alloy melted using the bottom mold as the crucible.

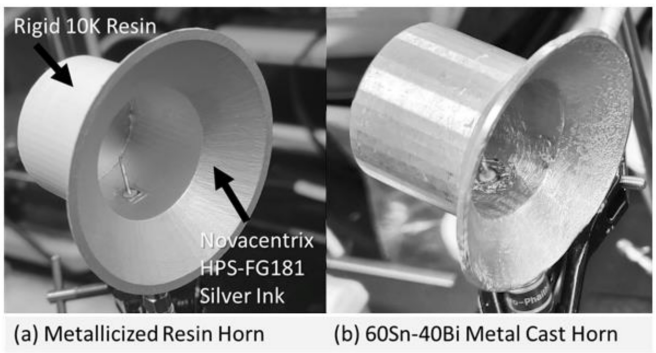

FIGURE 7. Fabricated conical horns.

Both the metallicized resin conical horn and the metal cast conical horn can be seen in Figure 7. The silver ink coating of the resin is applied on the inside surface as noted in the figure. The inside surface is the waveguide boundary. Both versions of the antenna have identical dimensions. For the metal cast horn, a hole was drilled to place the antenna feed and Sn-Bi solder used to affix the feed in the hole. Some sanding was done to the metal cast horn to remove burrs on the edges and make the edge surface smooth.

B. RESULTS AND DISCUSSION

As alluded to in the introduction, owing to relatively lower resistance one would expect the metal cast antenna to outperform the resin metallicized antenna. This expectation is attributed to losses in the silver conductive ink, which has a significantly higher resistivity than 60Sn-40Bi (which is

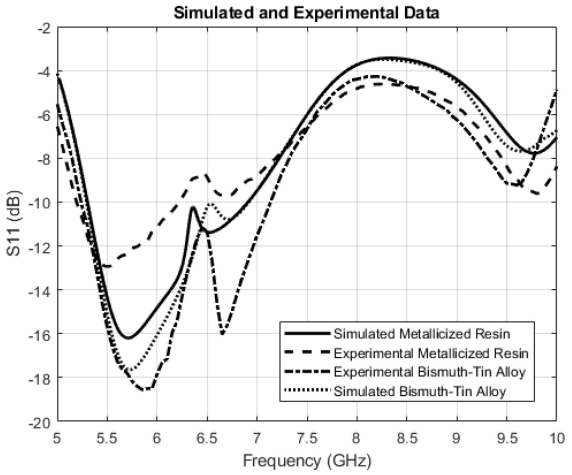

FIGURE 8. Simulated and experimental results for conical horns.

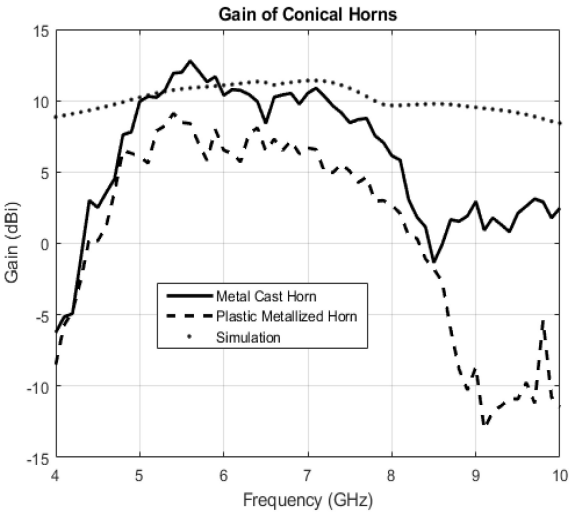

FIGURE 9. Measured and simulated maximum gain of conical horns as a function of frequency.

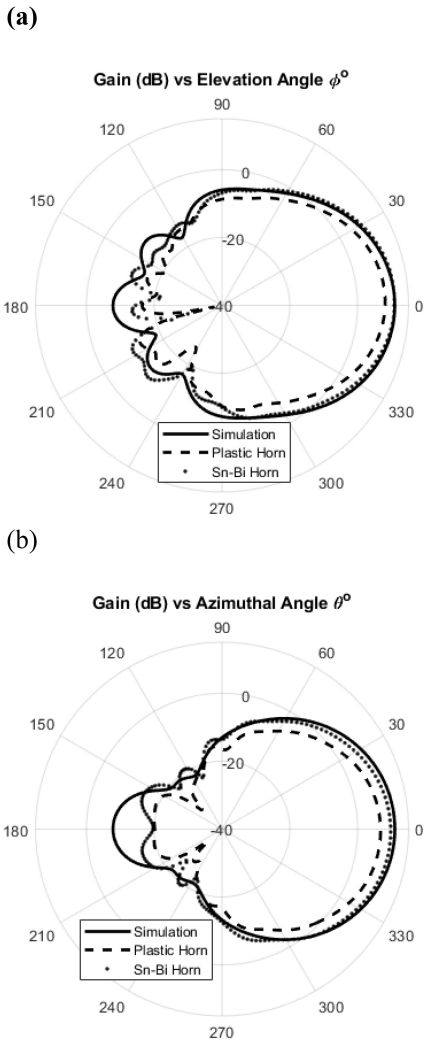

FIGURE 10. Simulated gain of horns at 5.8 GHz - (a) Measured and simulated gain of conical horn about the elevation. (b) Measured and simulated gain of conical horn about the azimuth.

0.383 $\mu\Omega$-cm [28]) in the cast variety and possibly to minor losses in the dielectric on which the silver is applied, as some of the wave leaks through the ink. The better performance of the metal cast antenna, shown in Figure 8 and Figure 9 is consistent with the expectations. The metallicized resin horn was resonant from 5.2 GHz to 6.2 GHz, while the metal cast horn was resonant from 5.2 GHz to 7.2 GHz. With a bandwidth of 2 GHz, the metal cast horn had twice the available bandwidth of the metallicized resin horn.

It was expected that the metal cast horn would have a better return loss and higher gain than the resin printed horn, due to the higher losses in the resin horn. It can be seen that both the simulated and experimental return loss for the metal cast conical horn is -18.5 dB in dominant mode and -13 dB in dominant mode for the resin horn. The gain of the metal cast antenna is also closer to what would be expected for a conventional conical horn with an aperture this small and approaches the simulated maximum gain of 12.5 dB. It is also worth noting that a simulated conical horn made of perfect electrical conductor (PEC) with the same dimensions is not significantly better than one simulated from 60Sn-40Bi. While the metal casting process is slightly more complex it did not take any more time than the curing time required for the resin process and led to better results. Furthermore, the price of both methods is reasonably low compared to the price of horns currently on the market.

Figure 10 shows the simulated and measured gain of the horns as a function of the azimuthal angle Theta and the colatitude Phi at 5.8 GHz for the horn. There is a significant difference in measured gain in the direction of highest directivity as a function of frequency between the metal cast and the resin horn. The lower gain of the resin horn compared to the metal cast horn as seen in Figure 9 is expected, due to the losses in the silver conductive ink. What is clear from the differences in simulation and measurement for the resin horn in Figures 7 and 8 is that there are significant losses in the silver conductive ink that are not accounted for

in simulation. The model used in simulation was based on the ideal case. However, this simplified approach overlooks the reduced conductivity of the ink compared to metal and materials that may include polymeric binders and conductive polymers as part of the silver conductive ink used to metallize the resin horn. These materials are often included to aid in keeping the silver conductive ink particles in electrical contact with each other and to make the inks mechanically stronger and more flexible. These polymeric binders and conductive polymers have their own permittivity, loss tangent and conductivity, which impact the experimental results of a real antenna [29].

V. CAPACITIVELY COUPLED DISK LOADED MONOPOLE

Here we present a modular antenna topology, a capacitively coupled disk loaded monopole, that allows for quick and easy change of network configuration, without any need for exposing the metallic components to the environment (presented with a different matching structure and a reflector in [30]). Modifying systems without exposing metallic components is especially useful in harsh and corrosive environments like the deck of a ship or in coastal cities, where salt water can quickly degrade materials if not properly sealed [31] after installation. Modular systems provide advantages to maritime operators and city planners allowing them to reuse previous infrastructure, when older systems are replaced. The disk loaded monopole presented here allows for these changes to be made quickly and easily via a resin embedded interchangeable portion that determines the operating band of the antenna. The topology is an example of the resin casting methodology presented in Section III, and was designed with this manufacturing technique in mind. In the following section we detail the design of the capacitively coupled disk loaded monopole designed to be configured over a range that includes 2.45 GHz WiFi and the 2.3 GHz amateur satellite band.

A. DESIGN AND CONSTRUCTION

An ideal version of this topology designed and simulated in air has a spacing between each disk of 1/16th wavelength, with the first disk connected to the feed pin 1/16th wavelength above the ground plane. The first and second disk, and third and fourth disk are capacitively coupled. The second and third disk are joined by a conducting wire. The radius of the first disk is 1/8th wavelength and each successive disk is 5% smaller. This design allows for a significant portion of the antenna that need not be attached, but instead, be situated in appropriate proximity and alignment to the feed. Using the disks allowed for enough reactive elements to easily tune input impedances on one conductor and resonant frequency on another, without having to change the size of the interchangeable slug, as depicted in Figure 11.

The immediately obvious problem with this design is that it is not realizable without introducing some other structure to support the floating elements. This was not an oversight, but an integral part of the complete design of the topology.

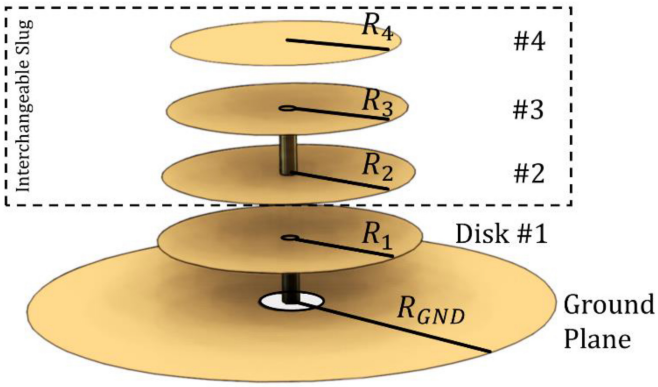

FIGURE 11. Capacitively coupled disk loaded monopole topology [30].

TABLE 3. Capacitively coupled disk loaded monopole design parameters [30].

Design Parameters	Dimensions by Material and Frequency		
	2.45 GHz In Air (mm)	2.45 GHz in Resin (mm)	2.30 GHz in Resin (mm)
r_{GND}	28.36	19.03	19.03
r_1	14.18	6.43	6.43
r_2	13.47	5.87	6.60
r_3	12.80	8.59	8.59
r_4	12.16	8.16	8.16
Disk Spacing	7.09	4.76	4.76
Pin Radius	0.89	0.60	0.60

The topology presented here is designed to be embedded in a dielectric substrate to completely isolate the metallic components from the weather. Embedding the antenna in resin with tunable capacitively coupled components allows for a reconfigurable structure that is ideal for marine and coastal environments, where salt water can have devastating effects on exposed metallic materials. This allows for reconfiguring exterior system components without damaging or replacing existing weather seals, thereby reducing the risk of corrosion and failure. Embedding the antenna in resin required only minor modifications to the design. Dividing all dimensions by the square root of the relative permittivity of the Formlabs' Rigid 10K resin (3.3) used as the dielectric produced a very close response. A parametric sweep in Ansys HFSS was used to finish tuning the parameters, which can be seen in Table 3. During the parameter sweep the feed disk size (r1) needed to tune the input impedance of the desired band of configurable frequencies was found to be

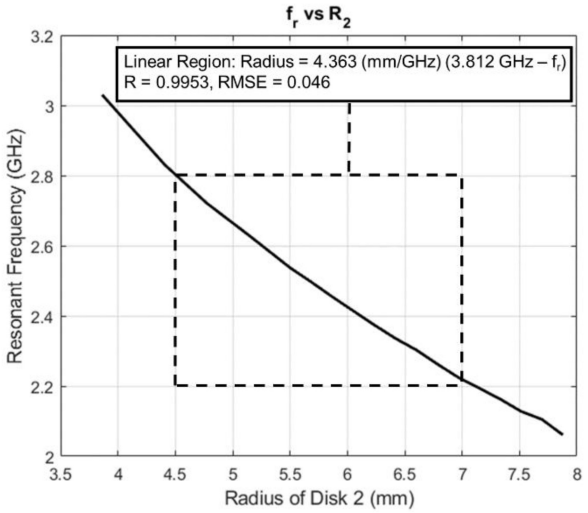

FIGURE 12. Resonant frequency as a function of tuning disk radius.

6.43 mm. Following that the linear relationship between resonant frequency and tuning disk radius (r2) was determined and can be seen in Figure 12. Because the tuning disk is in the interchangeable slug portion of the antenna it allows the antenna to be reconfigured by changing only the disks in the capacitively coupled portion of the antenna, which can all be placed in a small cylinder. Disks 3 (r3) and 4 (r4) are only scaled. Two such example configurations were constructed, one at 2.45 GHz WiFi and the other at the 2.3 GHz amateur satellite band.

One major design problem remained, which was significant reflection between the resin free space boundary. A numerical parametric study was performed to find the optimal matching structure geometry. There are several possible geometric solutions to this problem, but generally they all entail creating a gradient of effective permittivity to free space as a function of distance radially. Several dielectric matching structures were considered, however a wide biconical matching structure top loaded with a dielectric resonator resulted in the best performance (See Figure 13). The matching structure fits on top of the interchangeable slug, which rests on the ground plane and feed disk.

The antenna was designed such that the entire dielectric portion of the antenna could be easily molded using the resin casting methodology described in Section III. One such example of a cast part was produced for the interchangeable slug from Figure 13 b and 13 e. To save prototyping time the remaining parts were printed directly, but could also be easily cast in 2 or 3 part molds as well. The ability to produce molds by 3D printing supports fast production of the molds and fast prototyping of the antenna itself, while the molds allow for fast production at scale.

B. RESULTS AND DISCUSSION

Simulated results were compiled for several configurations for both S_{11} and Gain. Specifically, the S_{11} at each resonant frequency in the designed band of configurability (2.2 GHz

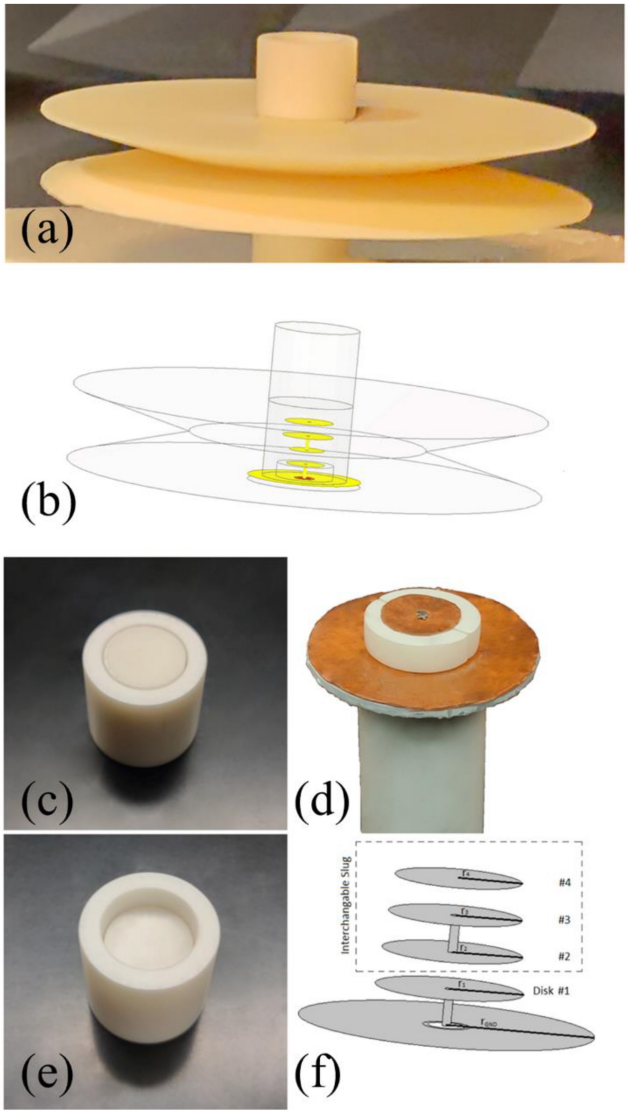

FIGURE 13. (a) Assembled capacitively coupled disk loaded monopole, (b) cad model with inside view, (c) interchangeable slug top, (d) feed disk, (e) interchangeable slug bottom, (f) general topology [30].

- 2.8 GHz) was recorded and plotted against the radius of disk 2 in Figure 14. This was done to confirm that the antenna's input impedance remained matched throughout its configurable band.

For the two example configurations 2.45 GHz and 2.3 GHz, S_{11} was simulated from 2 to 3 GHz. Measurements were made for this same band for both configurations and plotted against the simulated results as seen in Figure 15 a. There is good agreement between simulation and measurement in the S_{11} data for both configurations, with a larger difference seen in the 2.3 GHz configuration. The loss tangent of the Rigid 10K resin is unknown and is likely responsible for the difference between simulated and measured results. Simulated and measured results for gain in the 2.4 GHz configuration about the elevation angle are presented in Figure 15 b and about the azimuth in Figure 15 c. The antenna has cylindrical symmetry and radiation patterns

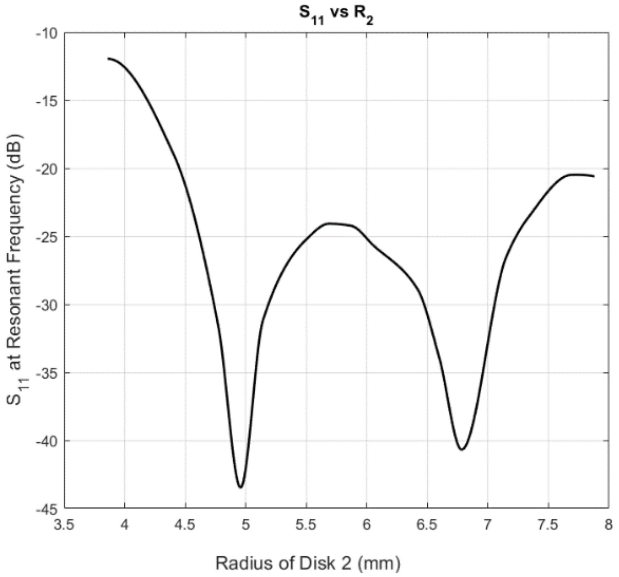

FIGURE 14. S_{11} at resonant frequency vs tuning disk radius.

TABLE 4. Capacitively coupled disk loaded monopole design parameters simulated maximum gain, directivity and radiation efficiency of 2.45 GHz and 2.3 GHz configurations.

Freq (GHz)	Peak Directivity (dB)	Peak Gain (dB)	Radiation Efficiency
2.45	3.40	3.40	1.00
2.30	2.98	2.57	0.91

in various configurations differ predominantly by maximum gain. The simulated maximum gain, directivity and radiation efficiency of both configurations are presented in Table 4. Bandwidth, directivity, gain and radiation efficiency are plotted in Figure 16 for all tuning disk radii in the linear band of configurability.

The results show that the capacitively coupled disk loaded monopole topology allows for an easily reconfigurable antenna, but more importantly it is an ideal showcase for the advantages of direct and indirect applications of additive manufacturing in antenna production. Direct printing of the dielectric materials allowed for rapid prototyping of the antenna, and rapid manufacturing of molds for mass production capabilities. Furthermore, additive manufacturing opens several doors when it comes to matching structures for antennas in different environments. This is especially true for soil probes and antennas used for concrete assessment [32], [33], [34]. The topology is a demonstration of how additive manufacturing can solve many material issues with antennas today, while still keeping production capacity in mind.

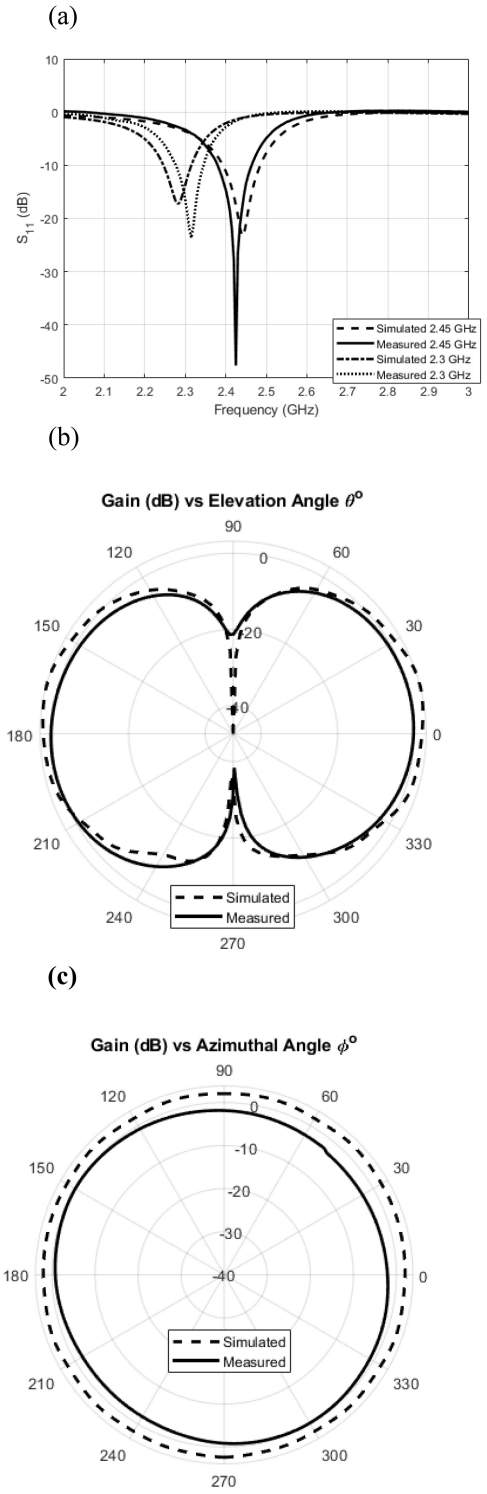

FIGURE 15. (a) Measured and simulated S_{11} of capacitively coupled disk loaded monopole, (b) Measured and simulated gain of capacitively coupled disk loaded monopole about the elevation at 2.45 GHz. (c) Measured and simulated gain of capacitively coupled disk loaded monopole about the azimuth at 2.45 GHz.

VI. CONCLUSION

In this paper, we presented two antenna fabrication methodologies that indirectly employ additive manufacturing. The first methodology presented cast low-melting temperature metals into additively manufactured molds made using a high temperature tolerating, glass-filled resin on an SLA printer. As an example of this methodology a conical horn

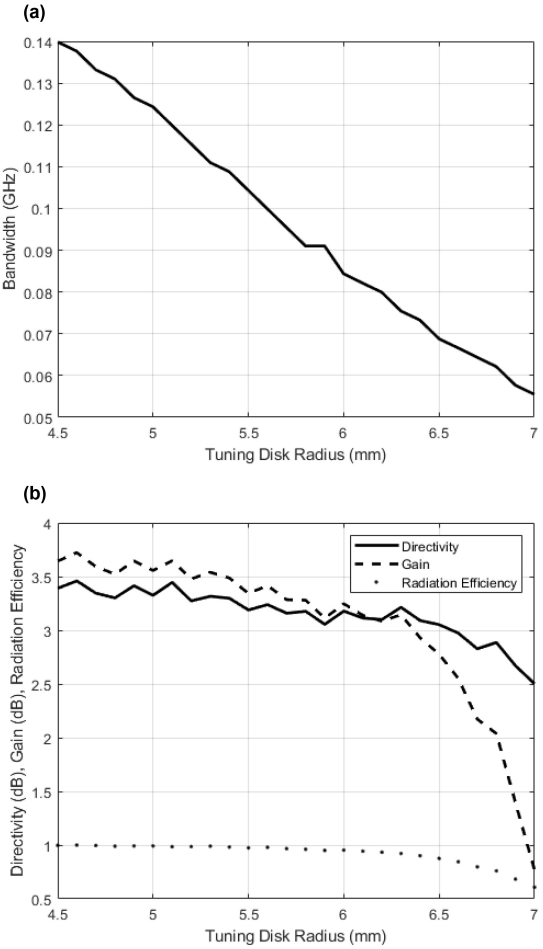

FIGURE 16. (a) Simulated bandwidth vs configured resonant frequency of capacitively coupled disk loaded monopole, (b) Simulated directivity, gain and radiation efficiency vs configured resonant frequency of capacitively coupled disk loaded monopole.

was fabricated and compared to a dimensionally identical horn constructed using a more traditional approach. The second methodology presented consisted of a multi-part casting process where a negative mold was created from PDMS cast into a clear SLA printed positive mold, whereupon the final part was created from casting the glass-filled resin into the PDMS negative. Parts from a capacitively coupled disk loaded monopole were used as an example of this fabrication methodology. The capacitively coupled disk loaded monopole has a complex topology and can benefit from the rapid prototyping afforded by additive manufacturing. Measurements for this topology were taken and compared to simulation in multiple configurations.

Measurements taken on the conical horns show an advantage in the metal casting methodology in performance compared to the metalized version while still reaping the same cost saving advantages shown in other additive manufacturing processes. This is achieved while maintaining the advantage of fast prototyping often attributed to additive manufacturing. Furthermore, for some geometries the metal cast molds may be reusable in part or full, thereby allowing for at scale production in a way that was not available with direct additive manufacturing methodologies. The resin casting methodology presented retained most of the benefits of additive manufacturing while allowing for completely reusable molds. This reusability provides a method of at scale production of dielectric component structures, while the use of additive manufacturing for the molds supports the ability to replace and update these parts quickly. Combining these two practices results in a process which can be optimized for both rapid prototyping and production at scale.

The presented capacitively coupled disk loaded monopole topology shows the versatility of additive manufacturing and how it can be used to produce configurable antennas specialized for a variety of physical environments. This physically reconfigurable topology allows for minimal effort to be expended in updating network requirements, while maintaining the weather seal for equipment in maritime environments; especially shipboard environments where the antenna may be the only component in the system outside the hull. Even outside of highly corrosive conditions, the ease of reconfiguration enables active development and testing in variable environments. The work presented here merges the benefits of additive manufacturing and casting methodologies to recast prototyping techniques into cost-effective, at-scale production capability.

REFERENCES

[1] B. Liu, Y. Wang, Z. Lin, and T. Zhang, "Creating metal parts by fused deposition modeling and sintering," *Mater. Lett.*, vol. 263, Mar. 2020, Art. no. 127252, doi: 10.1016/j.matlet.2019.127252. [Online]. Available: https://www.sciencedirect.com/science/article/pii/S0167577X19318841

[2] K. N. Paracha, A. D. Butt, A. S. Alghamdi, S. A. Babale, and P. J. Soh, "Liquid metal antennas: Materials, fabrication and applications," *Sensors*, vol. 20, no. 1, p. 177, Dec. 2019, doi: 10.3390/s20010177. [Online]. Available: http://dx.doi.org/10.3390/s20010177

[3] B. Ghassemiparvin and N. Ghalichechian, "Design, fabrication, and testing of a helical antenna using 3D printing technology," *Microw. Opt. Technol. Lett.*, vol. 62, no. 4, pp. 1577–1580, 2020. [Online]. Available: https://doi.org/10.1002/mop.32184.

[4] D. Helena, A. Ramos, T. Varum, and J. N. Matos, "Antenna design using modern additive manufacturing technology: A review," *IEEE Access*, vol. 8, pp. 177064–177083, 2020, doi: 10.1109/ACCESS.2020.3027383.

[5] R. Colella et al., "Electromagnetic analysis and performance comparison of fully 3D-printed antennas," in *Proc. Photon. Electromagn. Res. Symp. (PIERS-Spring)*, 2019, pp. 964–970, doi: 10.1109/PIERS-Spring46901.2019.9017888.

[6] J. Teniente, J. C. Iriarte, R. Caballero, D. Valcázar, M. Goñi, and A. Martínez, "3-D printed horn antennas and components performance for space and telecommunications," *IEEE Antennas Wireless Propag. Lett.*, vol. 17, no. 11, pp. 2070–2074, Nov. 2018, doi: 10.1109/LAWP.2018.2870098.

[7] A. T. Castro and S. K. Sharma, "A triple mode waveguide corrugated horn antenna using 3D printing technology," in *Proc. IEEE Int. Symp. Antennas Propag. USNC/URSI Nat. Radio Sci. Meeting*, 2017, pp. 1235–1236, doi: 10.1109/APUSNCURSINRSM.2017.8072660.

[8] B. Zhang, Y.-X. Guo, H. Sun, and Y. Wu, "Metallic, 3D-printed, K-band-stepped, double-ridged square horn antennas," *Appl. Sci.*, vol. 8, no. 1, p. 33, Dec. 2017, doi: 10.3390/app8010033. [Online]. Available: http://dx.doi.org/10.3390/app8010033

[9] U. Hasni, R. Green, A. V. Filippas, and E. Topsakal, "One-step 3D-printing process for microwave patch antenna via conductive and dielectric filaments," *Microw. Opt. Technol. Lett.*, vol 61, no. 3, pp. 734–740, 2019. Accessed: Oct. 20. 2022. [Online].Available: https://onlinelibrary.wiley.com/doi/pdf/10.1002/mop.31607

[10] V. T. Bharambe, J. Ma, M. D. Dickey, and J. J. Adams, "Planar, multifunctional 3D printed antennas using liquid metal parasitics," *IEEE Access*, vol. 7, pp. 134245–134255, 2019, doi: 10.1109/ACCESS.2019.2942058.

[11] D. C. Lugo, R. A. Ramirez, J. Castro, J. Wang, and T. M. Weller, "3D printed multilayer mm-wave dielectric rod antenna with enhanced gain," in *Proc. IEEE Int. Symp. Antennas Propag. USNC/URSI Nat. Radio Sci. Meeting*, 2017, pp. 1247–1248, doi: 10.1109/APUSNCURSINRSM.2017.8072666.

[12] N. Asnafi, T. Shams, D. Aspenberg, and C. Öberg, "3D metal printing from an industrial perspective—Product design, production, and business models," *Berg Huettenmaenn Monatsh*, vol. 164, pp. 91–100, Feb. 2019, doi: 10.1007/s00501-019-0827-z.

[13] Formlabs. "RIGID 10K material properties data." Jun. 2020. [Online]. Available: https://www.dynamism.com/media/catalog/product/pdf/Formlabs_Rigid_10K_TDS.pdf

[14] F. Wang, H. Chen, Y. Huang, L. Liu, and Z. Zhang, "Recent progress on the development of Sn–Bi based low-temperature Pb-free solders," *J. Mater. Sci. Mater. Electron.*, vol. 30, no. 4, pp. 3222–3243, 2019. [Online]. Available: https://doi.org/10.1007/s10854-019-00701-w

[15] A. A. Luo, A. K. Sachdev, and D. Apelian, "Alloy development and process innovations for light metals casting," *J. Mater. Process. Technol.*, vol. 306, Aug. 2022, Art. no. 117606.

[16] C. Sithole, K. Nyembwe, and P. Olubambi, "Process knowledge for improving quality in sand casting foundries: A literature review," *Procedia Manuf.*, vol. 35, pp. 356–360, Jan. 2019.

[17] M. N. A. Aziz, Rusnaldy, P. Munyensanga, S. A. Widyanto, and Paryanto, "Application of lost wax casting for manufacturing of Orthopedic Screw: A review," *Procedia CIRP*, vol. 78, no. 1 pp. 149–154, Oct. 2018, doi: 10.1016/j.procir.2018.08.304

[18] E. Alfonso, A. Haddadi, S. Carlsson, T. Emanuelsson, and J. Andren, "Developments towards the mass-production of high-gain GAP-based planar antennas for radio links," in *Proc. 12th Eur. Conf. Antennas Propag. (EuCAP)*, London, U.K., 2018, pp. 1–4, doi: 10.1049/cp.2018.0777.

[19] F. Bonollo, N. Gramegna, and G. Timelli, "High-pressure die-casting: Contradictions and challenges," *JOM*, vol. 67, no. 5, pp. 901–908, 2015.

[20] J. Campbell, "Perspective chapter: A personal overview of casting processes," in *Casting Processes and Modelling of Metallic Materials*. London, U.K.: IntechOpen Ltd., Feb. 2021, doi: 10.5772/intechopen.93739.

[21] X. Ye, H. Liu, Y. Ding, H. Li, and B. Lu, "Research on the cast molding process for high quality PDMS molds" *Microelectron. Eng.*, vol. 86, no. 3, pp. 310–313, 2009, doi: 10.1016/j.mee.2008.10.011. [Online]. Available: https://www.sciencedirect.com/science/article/pii/S0167931708004656

[22] American elements. "Product datasheet Bismuth Tin Alloy, BI-SN-01-P.40BI datasheet." Accessed: Dec. 2022. [Online]. Available: https://www.americanelements.com/bismuth-tin-alloy-12010–55-8

[23] Formlabs. "Compare formlabs dental 3D printer tech specs." Accessed: Oct. 25, 2022. [Online]. Available: https://dental.formlabs.com/products/form-3b/tech-specs/

[24] B. Venzac et al., "PDMS curing inhibition on 3D-printed molds: Why? Also, how to avoid it?" *Anal. Chem.*, vol. 93, no. 19, pp. 7180–7187, 2021, doi: 10.1021/acs.analchem.0c04944.

[25] I. Miranda et al., "Properties and applications of PDMS for biomedical engineering: A review," *J. Funct. Biomater.*, vol. 13, no. 1, p. 2, 2021, doi: 10.3390/jfb13010002.

[26] Formlabs. "BioMed clear resin technical data sheet." Jun. 2020. [Online]. Available: https://formlabs-media.formlabs.com/datasheets/2001432-TDS-ENUS-0.pdf

[27] Formlabs. "High temp resin material properties data." Jun. 2020. [Online]. Available: https://formlabs-media.formlabs.com/datasheets/1801087-TDS-ENUS-0P.pdf

[28] [G] American elements. "Bismuth Tin Alloy." Jun. 13, 2017. Accessed: Mar. 14, 2023. [Online]. Available: https://www.americanelements.com/bismuth-tin-alloy-12010–55-8

[29] T. Leng, X. Huang, K. Chang, J. Chen, M. A. Abdalla, and Z. Hu, "Graphene nanoflakes printed flexible meandered-line dipole antenna on paper substrate for low-cost RFID and sensing applications," *IEEE Antennas Wireless Propag. Lett.*, vol. 15, pp. 1565–1568, 2016, doi: 10.1109/LAWP.2016.2518746.

[30] J. Lundquist, L. Linkous, and E. Topsakal, "Mechanically configurable, capacitively coupled, disk loaded monopole driven corner reflector," in *Proc. U.S. Nat. Comm. URSI Nat. Radio Sci. Meeting (USNC-URSI NRSM)*, 2022, pp. 12–13, doi: 10.23919/USNC-URSINRSM57467.2022.9881449.

[31] K. R. Raghu, "Challenges of the naval electromagnetic environment for the EMC engineer," in *Proc. 8th Int. Conf. Electromag. Interference Compatibil.*, 2003, pp. 41–46, doi: 10.1109/ICEMIC.2003.237780.

[32] A. Woszczyk et al., "A modified open-ended probe as a reliable tool for measurements of soil water content," in *Proc. Baltic URSI Symp. (URSI)*, 2020, pp. 161–164, doi: 10.23919/URSI48707.2020.9254053.

[33] N. Dhingra, N. Saluja, V. Kanwar, and R. Garg, "Moisture sensitive electrical property measurement in concrete slab with step graded antenna," *Proc. Mater. Today*, vol. 45, pp. 5172–5176, Mar. 2021, doi: 10.1016/j.matpr.2021.01.695.

[34] M. Ozturk, "Embedded smart sensor dipole antennas for real-time damage assessment, humidity, and temperature monitoring in reinforced and non-reinforced concrete structures," *Int. J. Microw. Wireless Technol.*, vol. 14, no. 4, pp. 482–491, 2021, doi: 10.1017/S1759078721001409.